Parallel domain discretization algorithm for RBF-FD and other meshless numerical methods for solving PDEs

Matjaž Depolli[a,*], Jure Slak[a], Gregor Kosec[a]

[a]Jožef Stefan Institute, Jamova cesta 39, SI-1000 Ljubljana, Slovenia

Abstract

In this paper, we present a novel parallel dimension-independent node positioning algorithm that is capable of generating nodes with variable density, suitable for meshless numerical analysis. A very efficient sequential algorithm based on Poisson disc sampling is parallelized for use on shared-memory computers, such as the modern workstations with multi-core processors. The parallel algorithm uses a global spatial indexing method with its data divided into two levels, which allows for an efficient multi-threaded implementation. The addition of bootstrapping enables the algorithm to use any number of parallel threads while remaining as general as its sequential variant. We demonstrate the algorithm performance on six complex 2- and 3-dimensional domains, which are either of non rectangular shape or have varying nodal spacing or both. We perform a run-time analysis of the algorithm, to demonstrate its ability to reach high speedups regardless of the domain and to show how well it scales on the experimental hardware with 16 processor cores. We also analyse the algorithm in terms of the effects of domain shape, quality of point placement, and various parallelization overheads.

Keywords: parallel, point fill, meshless, Poisson disc sampling, performance

1. Introduction

Many natural phenomena can be described with partial differential equations (PDEs) that are in most practical cases unsolvable in closed form and numerical approaches are used instead. An important part of the whole numerical solution procedure is domain discretisation, i.e. a division of the domain of interest into small discrete parts. The simplest way to numerically address PDEs is to use the Finite Difference Method (FDM) where the domain is covered with equidistant orthogonal mesh that can be trivially constructed. Despite its simplicity, FDM can be a powerful tool for simple geometries; however, complications arise with irregular geometries or when performing adaptive refinement. A more advanced method is the Finite element method (FEM), a standard

---

*[*]Corresponding author

Email addresses: `matjaz.depolli@ijs.si` (Matjaž Depolli), `jure.slak@ijs.si` (Jure Slak), `gregor.kosec@ijs.si` (Gregor Kosec)

numerical tool for engineering and scientific simulations that solves PDEs in weak form. Although FEM is capable of solving PDEs on irregular domains and supports all types of adaptivity, meshing of realistic 3D domains itself remains a problem that often requires user assistance and thus cannot be fully automated [1].

As a response to geometrical limitations of simple methods like FDM and the complexity of meshing required by FEM, a new class of meshless or often also referred to as meshfree methods emerged [2]. The difference between the mesh-based and the meshless methods is in consideration of the relations between nodes. The mesh-based methods structure nodes into polygons that cover entirely the domain of interest, the process referred to as meshing. On the other hand, the meshless methods fully define the relation between nodes only by internodal distances. An important implication of this distinction is that the meshless methods can solve PDEs on a set of scattered nodes, without a mesh [1, 2]. The recent review on Taylor series expansion based methods discusses also the performance of strong form meshless methods in problems with non-smooth solutions [3].

In the early stages of meshless development, some authors communicated that completely arbitrary nodes, e.g. randomly generated, can be used in meshless methods [2], making node generation seemingly trivial. Today, it is widely accepted that despite meshless generality regarding the node positions, nodes have to be positioned with certain rules in mind [4]. Despite the limitations in node positioning, the discretisation of the domain with scattered nodes is still a less complex operation than meshing [4, 5].

In the last few years, a substantial effort has been put into the development of algorithms dedicated to the meshless discretisation, i.e. the node positioning algorithms. In general, there are different node positioning strategies ranging from expensive iterative relaxation algorithms [6, 7, 8], advancing fronts [9], to sphere packing algorithms [10]. Recently, the Poisson disc sampling (PDS) [11] based positioning algorithm that generate nodes suitable for a meshless numerical analysis has been proposed [4, 12]. In [4] the authors introduced the PDS based algorithm that places nodes with spatially variable nodal density in an arbitrary domain in two, three or more dimensions. The quality of generated nodes has been, after a thorough analyses, verified by solving a transient solution of a coupled heat and momentum transport (natural convection problem) in a complex 3D domain with Radial Basis Functions Generated Finite Difference (RBF-FD) method [13].

Encouraged by the results presented in [4, 14] the PDS based algorithm was promoted to a default discretisation algorithm for an open source meshless project Medusa [15]. Since its integration in Medusa, it has been used in high order solution of Poisson's equation, including a solution of a problem in 4D [16], and in an engineering simulations of overhead power thermal rating [17]. The algorithm has also been generalised to the discretisation of n-D parametric surfaces, an important step towards the coupling of meshless methods and Computer-Aided Design (CAD) [18]. Generating nodes on parametric surfaces could also be used in conjunction with a dedicated surface reconstruction algorithm [19] to numerically address problems on or within the geometry given by a real point cloud data, for which there is no guarantee that the points are distributed according to the requirements for meshless nodes.

The algorithm [4] inherently supports h-adaptive numerical analysis through the spatially variable node density that directly affects the internodal distance h. In adap-

2

tive approach, nodal density function is constructed in such way that in areas with higher expected error h is reduced and in areas with lower expected error h is increased. The crucial part in constructing appropriate nodal density function is error estimate that defines the refinement criteria. Error estimates have been in the meshless context researched to some degree both in weak and strong form solutions of elasticity problems [20, 21]. In the context of RBF-FD method a ZZ [22] type error indicator has been demonstrated in [23], and in meshless methods relying on the least-squares approximation residual based error indicator have been discussed in [24]. Recently, also a Partition-of-unity based error indicator has been demonstrated in adaptive RBF-FD solution of Poisson's equation [25]. Besides indicators that extract knowledge about the error solely from a numerical method, ad-hoc error indicators that interpret the physical solution have been reported in [26, 27]. The latter approach has been also implemented with the discretization algorithm at hand in a fully adaptive solution of elasticity problem [14], where the nodal density function has been constructed on top of data provided by ad-hoc error indicator.

Another important topic, especially in context of adaptive solution, is the selection of appropriate stencils from the point clouds. In context of RBF-FD the topic has been thoroughly investigated in adaptive solution of Poisson's equation [26], including the problems with point singularities [23]. In [28], the authors present a method for stencil selection, based on the visibility criterion, for convex, concave, and singular problems in 2D and 3D. In [26, 23] authors demonstrated effective stencils of 6 or 5 nearby points that are sufficiently uniformly distributed around central node to support RBF-FD, and successfully solved several test problems. Nevertheless, often a much simpler approach where a certain, e.g. 12 or more in 2D [16], number of closest nodes form a stencil is used. Although such approach is easy to implement and generalise to higher dimensions, it is worth noting that it is also computationally less effective, since more supporting nodes are required for stable computation, especially in adaptive approach.

Although the algorithm presented in [4] is computationally effective, it can become a computational bottleneck, especially as it cannot be executed in parallel, contrary to most of the other parts of the meshless solution procedure. It is therefore the goal of this paper to discuss the development of the parallel version of the PDS positioning algorithm presented in [4].

The PDS algorithm itself has been done in parallel before. In [29], where the authors partition the domain into independent cells and then groups cells in such a way that all the cells from the same group are sufficiently far apart to be sampled in parallel, without any conflicts. The algorithm trades some of the performance for the emphasis on the blue noise property of samples, a property not needed in the scope of meshless analysis. Although it supports non-rectangular domains and adaptive sampling, it does so on account of performance. The authors admit that the non-uniform sampling can be incredibly inefficient. In [30], PDS is parallelised, with the emphasis on blue noise consistency. The authors use the dart-throwing method to generate a large set of points that they prune later. Both dart-throwing and pruning can be done in parallel. Parallel pruning uses a location independent priority value given to every generated point to resolve the conflicts between concurrent processes. The performance is not satisfactory, though, since dart throwing is not efficient for non-rectangular domains, and the generation of a large number of additional points increases memory requirements and

processing overheads.

In this paper, we attack the problem differently to the aforementioned parallel attempts, since except for the parallelization, our goals are different. The goals are identical to the ones posed to the sequential algorithm in [4], namely a fast execution and enforced proper inter-nodal spacing, while the distribution of placed nodes is free to diverge from the blue noise pattern. We developed a parallel algorithm based on an advancing-front method, inherited from its sequential parent, which does not suffer performance penalties on non-rectangular domains and non-uniform sampling. However, parallelization options are limited for advancing-front algorithms, since addition of new points is constricted to areas covered by the open fronts. Therefore in the proposed algorithm, the main novelties are the partitioning step that enables creation of multiple fronts and the dynamic parallel spatial indexing that supports parallel manipulation of fronts.

The rest of the paper is organised as follows: in section 2 the sequential algorithm and its application in RBF-FD is discussed, in section 3 a parallel algorithm is presented, in section 4 experiments with the newly developed algorithm are given, followed by discussion in section 5; in the last section 6, conclusions and guidelines for future work are given.

2. Sequential algorithm

The algorithm operates on "points" in d-dimensional space, which are only referenced as "nodes" in the context of a numerical method. A domain $\Omega \subset \mathbb{R}^d$, a spacing function h, and n_s "seed points" $p_1, \ldots, p_{n_s}$ are taken as input parameters. The domain is assumed to be bounded and is represented with its characteristic function χ_Ω,

$$\chi_\Omega(p) = \begin{cases} 1, p \in \Omega \\ 0, p \notin \Omega. \end{cases} \tag{1}$$

The spacing function $h\colon \Omega \to (0, \infty)$ is assumed to be bounded away from zero, which ensures the finiteness of the algorithm. At least one seed point is assumed to be given for each connected component of Ω and all seed points are assumed to lie inside of Ω. Apart from that, there are no additional assumptions needed on the topological properties of Ω nor on the function h for the algorithm to work. Despite that, the algorithm is expected to work best if we also assume that the values of the spacing function h are at least an order of magnitude smaller than the sizes of geometric features of Ω, such as narrow choke points. This assumption is natural from the point of view of PDE discretisations, as any geometric feature must be properly discretised to solve the eventual problem. Similarly, the spacing function h is usually continuous, or even Lipschitz continuous, to produce gradual nodal spacing changes.

The algorithm works as an advancing-front algorithm and places points in a breadth-first-search manner, starting from the seed points. These are initially put in a queue, and the algorithm considers the points from the queue (also called "active" points) until the queue is empty. Besides the queue, the seed points are also inserted into a spatial index S. In each iteration, a point p is taken from the queue and expanded. That means that new candidate points $\{c_j\}_{j=1}^{n_{ct}}$ are generated from it, by placing them uniformly on

4

a d-dimensional sphere centred at p with radius $h(p)$. The newly generated candidates are then processed in sequence: if a candidate c lies outside Ω it is immediately discarded. Likewise, if c lies too close to any of the existing points, it is also discarded. This proximity check is performed by finding the distance to the closest neighbour of c using the spatial index S, and checking that the distance is smaller than $h(c)$. If the candidate c is not discarded by any of the tests, it is accepted, inserted into the queue and into the index S. The algorithm ends when the queue empties, and all the generated points are then contained in the index S.

The generation of candidates is done using the recursive discretisation of the d-dimensional sphere along the last spherical coordinate. The number of candidates is controlled using the parameter n_c, which represents the number of generated candidates on the great circle, and the total number of candidates n_{ct} is in the order of $O(n_c^{d-1})$, falling to the curse of dimensionality. The higher the number of candidates, the better the quality of the final discretisation. However, increasing the number of candidates comes with diminishing returns, and setting n_c between 10 and 30 is usually sufficient. Further details about the candidate generation and the sequential algorithm are available in the paper describing the sequential algorithm [4].

The time and space complexity of the sequential algorithm are best described in an output sensitive way, in terms of the total number of points n_p. The algorithm performs at most n_{ct} evaluations of χ_Ω and closest neighbour searches in S. Additionally, each point is inserted once, totalling n_p insertions in S, and the rest of the operations are (amortized) constant. The time complexity is thus

$$T_{\text{sequential}} = O(n_p T_I + n_{ct} n_p (T_\Omega + T_Q)), \tag{2}$$

where T_Q and T_I are time complexities of query and insertion operations in S, respectively, and T_Ω is the time complexity of evaluation of χ_Ω. For a practical implementation, it is usually assumed that T_Ω is constant, and T_I or T_Q are on average logarithmic in the number of points, such as when using a k-d tree for S. Therefore, the asymptotic time complexity of sequential algorithm can be simplified to:

$$T_{\text{sequential}} = O(n_{ct} n_p \log(n_p)), \tag{3}$$

The space complexity is bounded by how much space is needed in S to store n_p points. It depends on the spatial indexing used, but in case of k-d trees it is

$$S_{\text{sequential}} = O(n_p). \tag{4}$$

Figure 1 shows a sample execution of the algorithm. The test domain, which we shall refer to as "clover", is the area enclosed by the polar curve

$$r(\theta) = 3/2 - \cos^3(3(\theta - \pi/6)), \tag{5}$$

i.e.

$$\Omega_t = \{(x, y);\ x^2 + y^2 < r_p^2(\arg(x, y))\}, \tag{6}$$

where $\arg(x, y)$ represents the angle that the ray from the origin through point $p = (x, y)$ makes with the positive part of the x axis, or as commonly computed by the `atan2`

function. For demonstration we use spacing function

$$h_t(x, y) = h_{\min} + (h_{\max} - h_{\min})h_{\text{base}}(x, y), \tag{7}$$

$$h_{\text{base}}(x, y) = \cos^2(3 \arg(x, y)) \tanh(\sqrt{x^2 + y^2}), \tag{8}$$

where h is defined in such a way that it varies between the minimal spacing $h_{\min}$ and maximal spacing $h_{\max}$. The same test domain Ω_t and the spacing function h_t will be used throughout the paper. The number of placed points will be controlled by varying $h_{\min}$ and $h_{\max}$, but their ratio will be set to constant: $h_{\max}/h_{\min} = 5$, so that it can be visualised while being sufficiently complex to make the placement problem non-trivial. This domain showcases both irregularity and spacing variability, which can cause point placing algorithms to run inefficiently. At the same time, the domain is two-dimensional, which makes the visualisations much clearer. However, several three-dimensional examples are also included later in the paper.
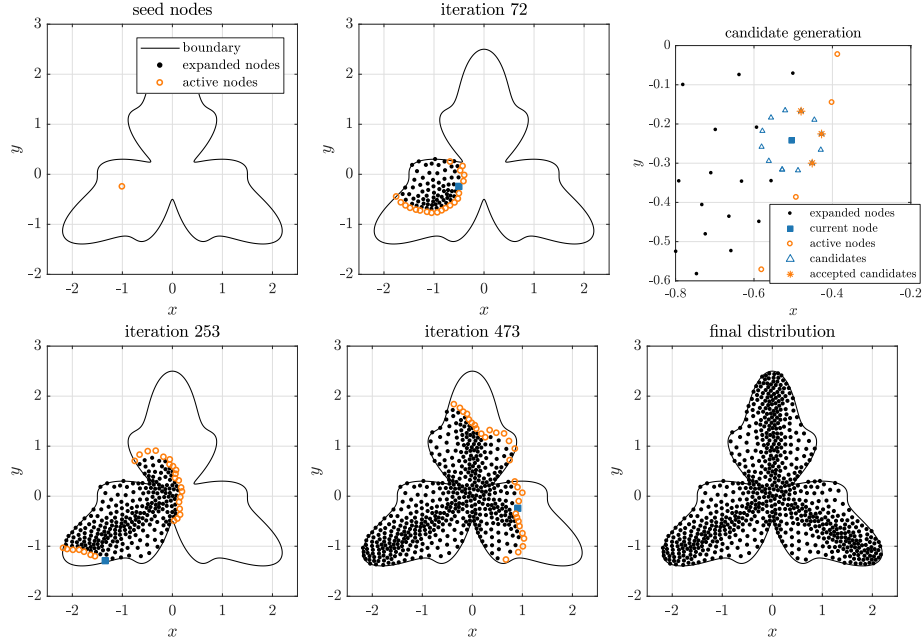
Figure 1: Execution of the point generation algorithm on the "clover" test domain, defined by Ω_t, with spacing function h_t and $n_c = 12$. The top right figure shows the candidate generation and selection around the "current point" in iteration 72.

2.1. Solving a PDE on scattered nodes

Although we focus on RBF-FD in this paper, the nodes generated with the presented algorithm can be used by any method that can operate on scattered nodes, such as Element-Free Galerkin (EFG) [31] or MLPG [1]. In our implementation of RBF-FD [32], the method expects the domain discretisation of a domain Ω in the form of

a list of nodes $X = x_1, \ldots, x_N$, some of which are in the interior, and some lie on the boundary of Ω. Each node x_i also has a list $I(x_i)$ of indices of its neighbours. The neighbours of each node constitute its stencil, and the stencils are usually computed as a part of the solution procedure. This is most often done by selecting some fixed number n of closest neighbours for each x_i (by Euclidean distance) and assigning their indices to $I(x_i)$. While node positioning on the boundary and in the interior is done with a dedicated algorithms, stencil selection is often a simple query operation on the spatial index.

As an example, we consider the following boundary value problem

$$\nabla^2 u = 0 \text{ in } \Omega \tag{9}$$

$$u + \alpha \frac{\partial u}{\partial \vec{n}} = u_a \text{ on } \Gamma_r \tag{10}$$

$$u = u_b \text{ on } \Gamma_d \tag{11}$$

that represents a steady-state temperature distribution in domain Ω, shown in Figure 2. The domain Ω represents a heatsink, obtained from [33], and Γ_d denotes the flat surface at the bottom of heatsink, at roughly $y = 2.5$ cm, and Γ_r is the rest of the domain's surface. The surface Γ_d is heated to a constant temperature of $u_b = 80\,°C$, and the rest of the surface experiences a flux proportional to the difference between the surface temperature and the ambient temperature $u_a = 20\,°C$, with the proportionality constant $\alpha = 200$ cm.

One of the solutions u is shown in Figure 2. This particular solution was obtained using $N = 214458$ discretisation nodes, of which 176896 were in the interior. Stencils of $n = 35$ closest neighbours were used, as well as Polyharmonic RBF $\phi(r) = r^3$ and augmentation with monomials up to 2nd order. Ghost nodes were used to handle Robin boundary conditions.
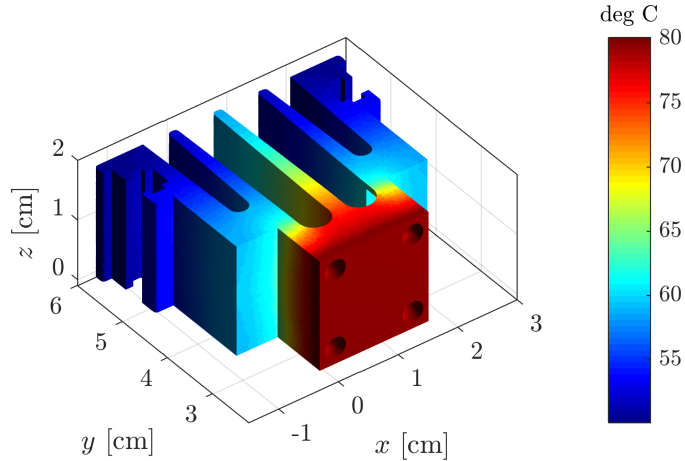
Figure 2: Temperature distribution in a heatsink, obtained by solving (9) through (11) using RBF-FD with sequential execution.

To determine the parallelisation opportunities, we separately measure each step's

execution time of the solution procedure. These steps include placing the points on the boundary, placing the points in the interior, computing stencil nodes, computing stencil weights, assembling the global linear system, and solving it. Figure 3 shows the proportion of the total running time that each of the parts takes for discretisations of different densities.
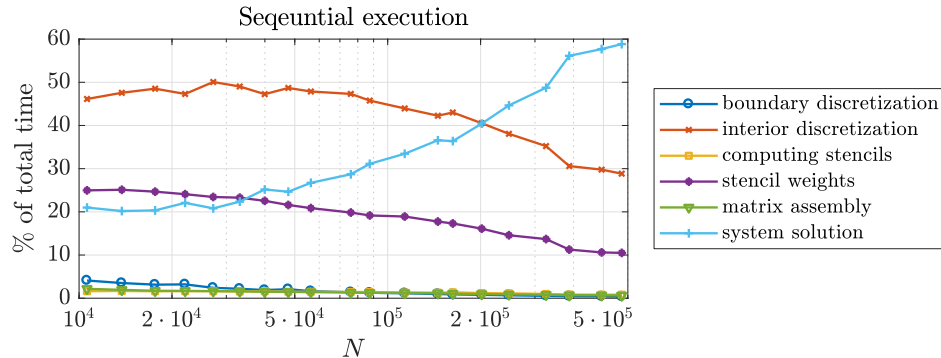
Figure 3: Distribution of running time between the parts of the solution procedure.

The most time-consuming parts of the solution procedure are the solution of the final system, the computation of stencil weights, and the point placing in the interior. All of these are worth parallelising. In fact, computing stencil weights can be trivially done in parallel, as computations for each point are independent. Parallelisation of linear system solvers is a whole research field of its own, with several implementations readily available online. The final part is the parallelisation of the node positioning algorithm, which is the focus of this paper.

3. Parallel algorithm

The development of a parallel algorithm started from the sequential version. We first analysed the sequential algorithm and found the following:

1. There are no parallel opportunities worth exploring within a single point expansion.
2. Expansions are prospective as units of parallel work.
3. Expansions of points are local in the sense that they do not require knowledge of the whole global state, i.e. all of the placed points, but only their immediate neighbourhood.
4. Expansions of p_1 and p_2 can be done concurrently if points are distant enough, i.e., distance between points p_1 and p_2 exceeds $\max(h(p_1), h(p_2))$.

We use these findings to design the parallel algorithm implemented as a set of sequential algorithms working in parallel. These sequential algorithms are transformed into threads, running on a single computer, sharing a global spatial indexing structure. For the threads to run independently, they should operate on distant points; therefore, they start from distant seed points. Such seed points are not readily available and must

be generated from the user-supplied seed points in a pre-processing step. This step is described in more detail in subsection 3.1. Next, the spatial indexing method is modified to allow concurrent insertions of distant points. It is divided into two levels, with seed points inserted into the top-level index and all other points inserted into the bottom level sub-indices. The top-level can be made read-only and thus thread-safe for the stage in which the bulk of points is inserted. The bottom level must use a synchronisation mechanism for the points to be correctly inserted, but this mechanism can be location-aware. The global spatial indexing structure is described in more detail in subsection 3.2. The overall pseudocode of the algorithm is presented in Algorithm 1 with the details explained in the following subsections.

> **input** : Domain Ω
> **input** : Nodal spacing function h defined on Ω
> **input** : A list of initial seed points X_{input}
> **input** : Number of seed points to generate, n_s
> **input** : Estimated number of points to cover the whole Ω: n_p
> **output:** A list of points X
> **begin**
>   **global** $X \leftarrow \{\}$;   // Location-aware indexed list of points.
>   // Partition the domain (bootstrapping step).
> $d \leftarrow$ dimensionality of Ω ;
> $a \leftarrow (n_p/n_s)^{1/d}$;
> $h_{\text{bootstrap}} \leftarrow a \cdot h$;
> $s_b \leftarrow$ new Sequential algorithm ;
> $X_{\text{seed}} \leftarrow s_b(\Omega, h_{\text{bootstrap}}, X_{\text{input}})$;
>   topLevelIndex$(X) \leftarrow X_{\text{seed}}$
> $\{X_{\text{seed},1}, ...X_{\text{seed},n_p}\} \leftarrow$ partition(X_{seed}, n_p) ;   // divide equally into n_p partitions
>   // Parallel fill
>   **parallel forall** $i_p \in [1, n_p]$ **do**
>   start thread$_i$;
>   **with** *thread$_i$* **do**
>   // Run sequential fill on predefined structures.
> $s \leftarrow$ new Sequential algorithm ;
>   point s.spatialIndexing to X ;
>   redirect s.output to X ;
>   sequential$(\Omega, h, X_{\text{seed},i})$
>   **end**
>   **end**
> **end**
> **return** X

Algorithm 1: The proposed parallel algorithm.

3.1. Bootstrapping

When designing algorithms optimised for efficiency, sometimes additional requirements and conditions on the input data are imposed, relative to the simpler algorithm's requirements and conditions. If those requirements can be relaxed by adding a pre-processing step to condition the input data without external help, we can call this step bootstrapping. In the case of the presented parallel algorithm, the input seed points can be insufficient in number (one per thread is required) and in their spacing (they should be as distant as possible to maximise concurrency). Therefore pre-processing is aimed

at generating a better set of seed points. This step's goals are very similar to the goals of the fill algorithm itself but with a much lower number of points to place. So, how could the fill algorithm be modified to bootstrap itself?

The main idea for placing several seed points is simple. For pre-processing, the algorithm should be executed exactly as for the main processing, using only a different spacing function $h_{\text{bootstrap}}$. To reduce the number of placed points down to the target number of seed points and to keep relative point density distribution unmodified, the spacing function should be linearly amplified: $h_{\text{bootstrap}} = a \cdot h$. The amplification factor a is used to linearly reduce the number of placed points per unit of d-dimensional volume. It can therefore be written as

$$a = (n_p/n_s)^{1/d}. \tag{12}$$

Note that the total number of placed points is usually not known exactly and can only be estimated and that the amplified spacing function cannot capture gradients in point density on the same level of detail as the original can. These two factors will cause the algorithm to "miss" the target number of seed points in most cases, but the number of placed points should still be close to the required number.

The generated seed points can be used to partition the domain Ω into sub-domains Ω_i we call cells, because of their similarity to the Voronoi cells. A cell Ω_i, defined by a seed point p_i, is the area containing those points from the domain that are closer to p_i than to any other seed point:

$$\Omega_i = \left\{ x; \ \|x - p_i\| = \min_{\substack{j=1,\ldots,n_s \\ j \neq i}} \|x - p_j\| \right\}. \tag{13}$$

The division into cells can then be used for location-aware synchronisation of the global spatial indexing. An example of division is shown in Figure 4. Note that even though the goal was to generate 4 seed points for 4 threads on the given example, the bootstrapping resulted in 7 seed points. It is trivial for the algorithm to use more seed points than threads, so such a result is perfectly acceptable.

3.2. Global spatial indexing

As explained before, spatial indexing is divided into two levels. The two levels differ by the type of points they hold; the top-level is for seed points, while the bottom level is for all other points. The top-level index S_{top} is generated during the bootstrapping phase, using a sequential algorithm. It is then made read-only – the points it holds define the cells, which form the base of the bottom level and may not be modified during the algorithm's execution. The bottom level is divided into as many sub-indices as there are seed points. Each sub-index S_i is used to index the space covered by its cell Ω_i. Sub-indices can also be thought of as branches if spatial indexing is performed by a k-d tree. The illustration of the two-level spatial index is shown in Figure 5. Note that the illustrated modifications can be applied regardless of the spatial indexing method used, which was k-d tree in our case.

Using the global spatial index, the procedure for placing a candidate point c is transformed as follows. First the nearest neighbour p_{nn} of c is found among the seed
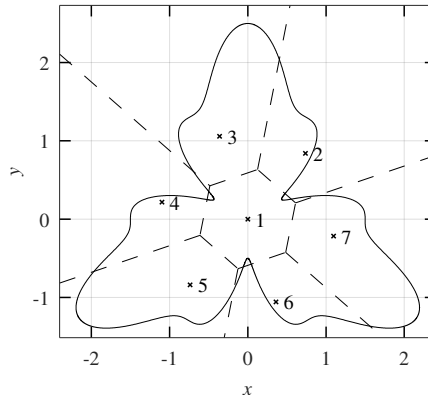
Figure 4: The clover domain divided into cells by the application of bootstraping. Cell borders are plotted with a dashed line. Centre points of cells, marked by ×, are seed points.

points on the top-level index. This can be done concurrently for any number of threads since the index is read-only. The neighbour p_{nn} determines the cell Ω_{nn} and its spatial index S_{nn} in which the proximity check for the c is then completed. If successful, c is added to the set of active points and indexed in the same spatial index, S_{nn}. Access to S_{nn} is synchronised with the use of a readers-writer lock to protect the index's shared state between a search and insertion. Readers-writer lock (also called single-writer or multi-reader lock) [34] is a locking mechanism that allows an unlimited number of concurrent readers but exclusive access for writers. Concurrent modification to S_i and S_j, however is possible when $i \neq j$. This is the main property that allows the fill algorithm to achieve high parallel efficiency.

The two-level spatial index can also be used as an additional result of the fill algorithm, for example to aid in computation of stencils. It can be used in the same way the traditional spatial index would be, as an immutable structure that is used for efficient search of n nearest neighbours. Procedure for searching one or more nearest neighbours in a two-level spatial index is comparable to that in a single-level spatial index. Although it is performed in two steps, one for each index level, the total number of operations is comparable. For example in k-d trees, to reach an element in the leaf, the combined depths of top-level tree and one of the lower-level trees have to be traversed, which sum up to approximately the total depth of a regular k-d tree index. Furthermore, when used only for searching, the two-level index can be safely used in parallel without a locking mechanism.

3.3. Advancing fronts

A single thread of the parallel algorithm performs an advancing front algorithm and will place points locally around the seed point. If more than one seed point is assigned to a thread, then such a thread will be advancing more than one front, but all the fronts will be localised to their starting cells in the beginning. Threads are oblivious to the details of the global spatial indexing and are not aware of which cell they are working

11
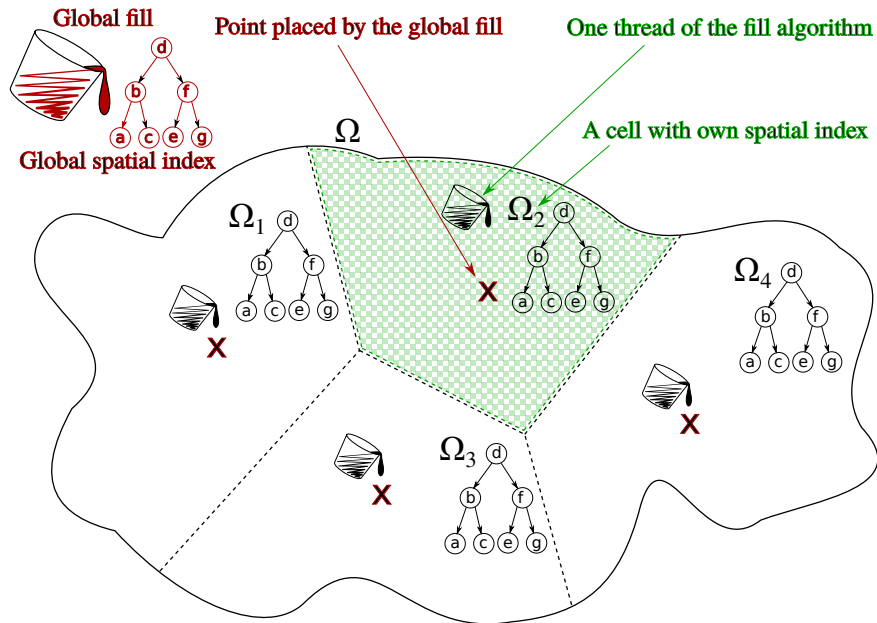
Figure 5: A fictional domain divided into cells. Individual fill threads are represented by buckets and spatial search indexes as binary trees.

on at any given moment. Fronts will thus, in time, cross cell borders unimpeded and enter neighbouring cells.

The efficient use of this method depends on the threads operating on different cells. While this is prescribed at the beginning when they operate on different seed points, it is no longer guaranteed after fronts cross cell borders. Eventually, parts of fronts will enter other cells and distribute threads' workload among more than just their starting cells. Two or more threads will sometimes try to enter critical sections of the same spatial index simultaneously and will be stopped by locks, introducing wait times that will lower the overall algorithm efficiency. It will be difficult for more than a few threads to be locked out and idle at any given moment in time, though, since their workloads will be distributed across many cells.

In Figure 6, an example of algorithm execution is shown. Note again that although the cell borders are marked in the figure, these are not known in advance, and only cell centres are available to the algorithm. On the presented example, where the number of threads, which is 4, is not a multiple of the number of seed points, which is 7, seed points are distributed among the threads unequally. Three threads start with 2 seed points each, while one starts with a single seed point. Thread 1 only gets seed point 1 and starts advancing a single front. The other three threads initially start with two advancing fronts each, which can be seen to collide for all three threads in Figure 6c). The same figure also shows how the fronts advance over the borders of cells.
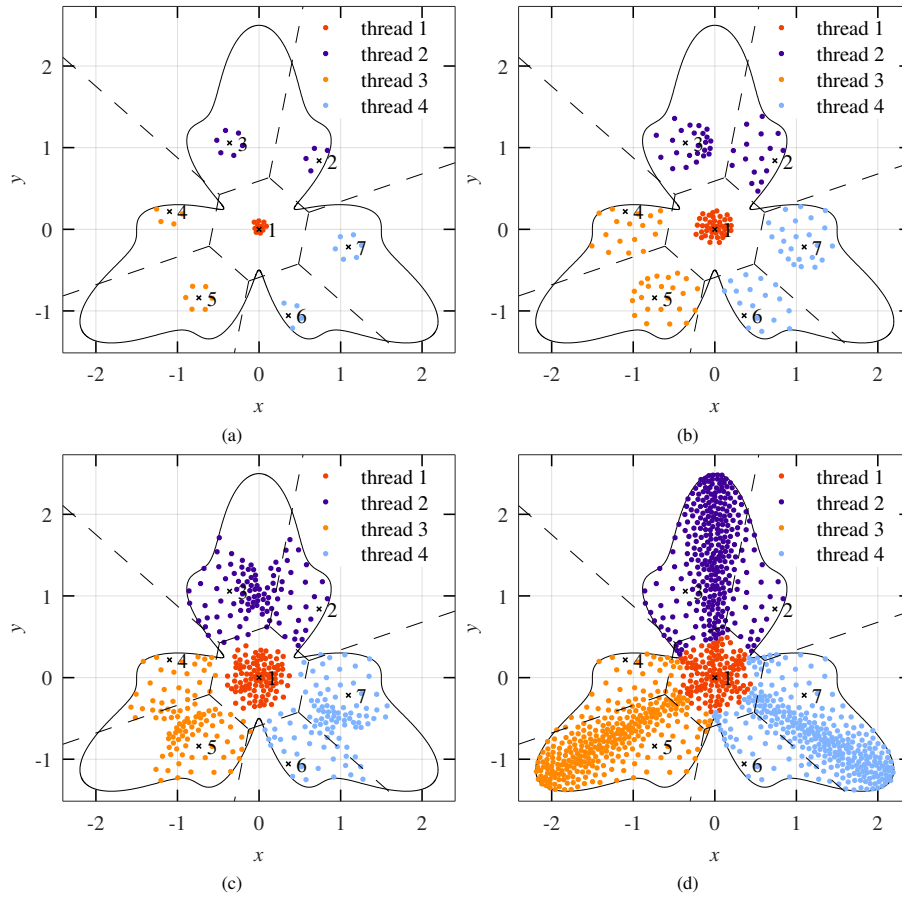
Figure 6: The clover domain filled with 4 threads and divided into 7 seeds by the bootstrapping. On all figures, the domain border is plotted with black continuous line, cell borders with black dashed line, and seeds by black crosses. Four snapshots of the algorithm are depicted: after each thread places 10, 40, 100 points, and after the algorithm finishes.

13

3.3.1. Computational complexity

We define the time complexity relative to the sequential algorithm complexity $T_{\text{sequential}}$ from (3). The parallel algorithm complexity can be constructed from equation

$$T_{\text{parallel}} = T_{\text{single thread}} + T_{\text{thread}} + T_{\text{bootstrap}}, \tag{14}$$

and we explain the additional elements below. $T_{\text{single thread}}$ is the execution time of the longest running worker thread. The worst-case scenario can be conceived where a single thread does all the work, and therefore this time is a sum of $T_{\text{sequential}}$ and the overhead of mutex acquisition. The latter is bounded by the number of candidate points considered, is constant per point, and is, therefore, $O(n_{ct}n_p)$. This is of a lower order than $T_{\text{sequential}}$, an thus $T_{\text{single thread}} = \Theta(T_{\text{sequential}})$. Thread management overhead is specified as T_{thread}, which depends linearly on the number of threads p and is constant per thread, thus $O(p)$. Finally, $T_{\text{bootstrap}}$ is the bootstrap overhead, which equals the execution of the sequential algorithm for placing the given number of seed points: $O(n_{ct}n_s \log(n_s))$. We can further assume a linear relation between n_s and p and therefore write that $T_{\text{bootstrap}} = O(n_{ct}p \log(p))$. Combining the elements of the equation gives:

$$\begin{aligned} T_{\text{parallel}} &= O(T_{\text{sequential}} + p + n_{ct}p \log(p)) \\ &= O(n_{ct}n_p \log(n_p) + n_{ct}p \log(p)), \end{aligned} \tag{15}$$

which is worse than the complexity of sequential algorithm. This result demonstrates that in the worst-case scenario, the proposed parallel algorithm could be very inefficient. An example of such a case is difficult to imagine though. The domain shape and its nodal spacing function would have to be degenerate to the point of not being useful for a numerical approach at all. While it seems improbable that such domains would be created and used by a human user, they could be created by an automatised method for optimisations or statistical calculations and should not be entirely disregarded.

To arrive at a more realistic estimate of complexity, we start with an assumptions of $p \ll n_p$, equally fast processor cores, and $T_{\text{single thread}} = T_{\text{sequential}}/p$. The latter is in line with the assumption listed already for the sequential algorithm, i.e. that the values of the spacing function h are at least an order of magnitude smaller than the sizes of geometric features of Ω. This pair of assumptions ensures that bootstrapping generates sufficiently distant seed points for the static load-balancing to work well enough. Then the time complexity of the parallel algorithm from (15) can be rewritten as:

$$T_{\text{parallel}} = O(n_{ct}n_p \log(n_p)/p + n_{ct}p \log(p)). \tag{16}$$

The spatial complexity becomes bounded by how much space is needed to store n_p points across a number of spatial indices S_i, and by the overhead of thread management, which is $O(p)$. In case k-d trees are used for spatial indexing, the space complexity is $O(n_p/p)$ per each of the p spatial indices and the space complexity becomes:

$$\begin{aligned} S_{\text{parallel}} &= O(pn_p/p + p) \\ &= O(n_p). \end{aligned} \tag{17}$$

14

4. Experiments

In this section, we experimentally evaluate how well does the presented parallel algorithm work on multi-core hardware. We define a set of experiments to evaluate the scalability as a function of a number of threads and problem size. A number of threads is used on a range that is available on the experimental hardware, $p \in [1, 32]$. Problem size is defined by the total number of points placed n_p and will range in our experiments from 1000, increasing by a factor of 4, up to 16 million. Note that our experiments only place approximately the given number of points, the exact number depending on the random seed, the number of threads, and positions of user-defined seed points. Therefore we shall talk about the "target" numbers of points, i.e. the number used to calculate the domain spacing function parameters in a way that should result in approximately that many points placed. The functions for calculating the spacing function parameters were manually preliminary fitted to several executions of the algorithm on several problem sizes. This was done offline and is out of the scope of the article. Note that the execution times were normalised with the actual number of placed points to remove the bias originating in a slightly varying number of points placed by the different runs for calculation of speedups.

4.1. Experimental setup

A computer based on a AMD Threadripper 2950X, a 16-core 32-thread processor and 32 GB of RAM was used to perform the presented experiments. The double thread count with respect to the number of cores is the consequence of the processor's simultaneous multi-threading ability (SMP), which allows a single physical core to execute two threads concurrently. The computer was running Ubuntu 20.04 desktop and was kept idle apart from running the experiments. As the majority of modern CPUs, the 2950X is capable of changing its clock frequency on per-core basis in real-time, on the one hand, to ensure maximum performance, and on the other hand, to limit power usage and keep die temperature within safe bounds. To measure the speedup on equally powerful CPU cores, regardless of how many cores are in use, we have disabled the dynamic frequency boost and set a fixed frequency of 2.2 GHz for all cores. Furthermore, we used thread binding in all our experiments, which means that the number of threads always matches the number of used cores, since each thread is bound to a single core, and there is at most one thread per core. Here we also count the virtual cores, i.e. the use of SMP results in Linux seeing the number of cores as twice the number of physical CPU cores. These virtual cores are numbered from 17 to 32, and we use them only for experiments with 17 or more threads. Not using these cores on a lower number of threads improves the use of local core caches, and thus the performance of the proposed algorithm can nearly fully utilise any core with a single thread.

All the presented algorithms were implemented in C++, using its standard library for multi-threading (`std::thread`). Threads were created with C++ lambda expressions, which deferred the call to a member function on a pre-constructed object instance. The end of thread execution was detected with the `std::thread::join` function, which suspends the waiting thread until the target thread completes. Mutexes of class `std::shared_mutex` were used, which implement two levels of access protection - shared and unique, which makes it possible to protect critical sections of code

with readers-writer locks. The spatial indexing was performed using a mature and heavily optimised library "nanoflann", which supports both statically and dynamically constructed *k*-d trees [35]. For the top-level index, a statically built tree was used, while for the bottom level sub-indices and for the sequential algorithm, the dynamically built trees were used.

4.2. Speedup

Speedups from all the performed experiments, computed relative to the sequential algorithm, are shown in Figure 7. There are several main observations possible from this figure. Foremost, the speedups are significant, especially for the large problem sizes. Moreover, they are mostly increasing up to 16 threads, which is the number of cores on the computer used, and nearly linear for the low number of threads. The use of additional threads, available due to the processor's support for SMP, ranges in effect from slightly hindering performance to slightly boosting performance. The likely cause of this is that the algorithm's workload is not diverse enough for SMP to be able to run two threads on the same core efficiently. Running the algorithm on 17 threads, for example, thus loads physical core 1 with two threads and all the others with only one, and thus makes the two threads on core 1 run appreciably slower than the rest. The effect of this is detrimental since the algorithm assumes equally fast execution on all threads, which no longer holds in the described situations. A dynamic load balancing could be implemented to tackle this issue, but this is beyond the scope of the presented algorithm. In further tests and discussions, we focus mostly on the performance when all physical cores are loaded, that is, at 16 threads

It is also very apparent that placing even a very low number of points can be sped up using multi-threading, and the only instance of the problem which does not scale well to at least 16 threads is 1000 points. More substantial speedups are only achievable when several ten thousand points are to be placed, and the best-achieved result in the shown experiments was a speedup of 12 at 16 threads. To get a better feeling for the problem sizes, it takes the sequential algorithm 12 ms to place 1000 points and 230 s to place 16 million points.

4.3. Domain shape and spacing

Eight domains are used to demonstrate the robustness of the algorithm. These domains can be classified into four pairs: "heatsink", "clover", "bunny" and "maze", each in 2-D and 3-D version. The 2-D domains are shown in Figure 8 and 3-D domains in Figure 9. The 2-D clover domain was already used in visualisations of the algorithms and the 3-D heatsink is the domain used in Section 2.1. The 3-D heatsink is the only domain which is not homeomorphic to a sphere.

Both heatsink domains are used in conjunction with the uniform point spacing, which seems optimal for the demonstrated simulation of heat transfer. Since non-uniform nodal distributions are often used in real-life domains and are also often the source of performance loss in other node placement algorithms, we have devised non-uniform spacing functions for the other 6 domains.
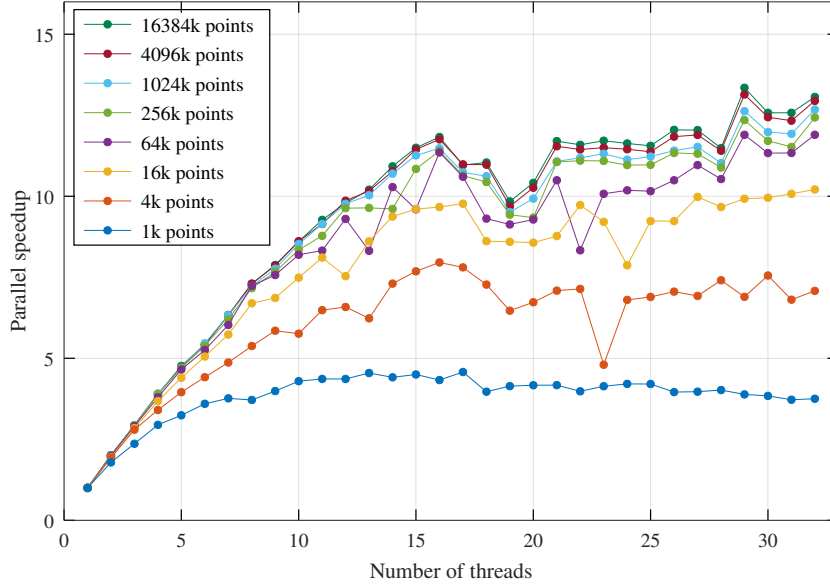
Figure 7: The speedup of the cell-based parallel algorithm as a function of the number of threads for several problem size levels, defined by the number of placed points. All the results were obtained on the 2-D clover domain.

The boundaries of both 2-D and 3-D versions of clover are defined in closed form, with 2-D defined in (6) and 3-D given as a surface in spherical coordinates as

$$r_{\text{clover-3D}}(\phi, \theta) = \frac{3}{2} - \cos(3(\phi - \pi/6))^3 (\pi - \theta)^2 \theta^2 / 8, \quad \phi \in [0, 2\pi), \ \theta \in [0, \pi]. \quad (18)$$

Both versions of clover are also star-shaped with respect to the origin, which allows us to easily define the characteristic function by just checking the inclusion radius.

The rest of the domains are polytopes. The 3-D bunny is a watertight version of the standard Stanford bunny model [36]. The 2-D version was drawn manually in InkScape, from where the coordinates were also exported. The bunny domains are used to showcase the behaviour of the algorithm on realistic 2-D and 3-D objects. Both of the maze domains are meant to explore the behaviour of the algorithm on more complex structures. The 2-D version was generated using a quick recursive-backtracking maze generation algorithm, and the 3-D version was generated using [37] with some post-processing in Meshlab. The 2-D heatsink domain is the projection of 3-D heatsink on the *xy*-plane.

Spacing functions for the presented domains are defined in table 1.

Equation for the 2-D clover spacing function is derived from (7), by requiring $h_{max}/h_{min} = 5$, and then replacing h_{min} and h_{max} with a single scaling parameter h_s. The latter is used to adjust for the total number of placed points, as required by the experiments. Similarly all the other spacing functions have a fixed maximal to minimal value ratio and use a single scaling parameter. Spacing function for both heatsink

17

(a) 2-D clover

(b) 2-D heatsink

(c) 2-D bunny

(d) 2-D maze
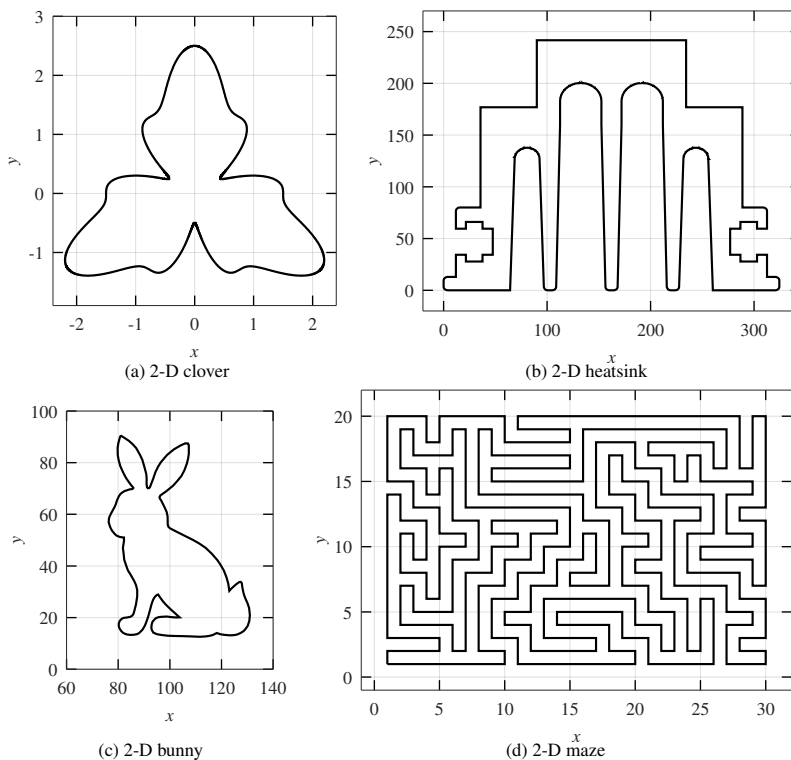
Figure 8: 2-dimensional test domains.

domains comprises only a scaling factor, since these two domains employ a uniform spacing.

We plot one resulting set of scattered nodes for each domain, with colours of the points corresponding to the threads that placed them. The 2-dimensional domains were filled with a target $n_p = 4000$ points and are presented in Figure 10. The 3-dimensional domains were filled with a target $n_p = 16000$ points and are presented in Figure 11. The parameters common to all sub-figures are $n_c = 12$, $p = 16$, $n_s = 32$, and the use of bootstrapping to generate seed points from a single internal seed point. The visualisations of the results show no visible deficiencies, all the domains are filled with points as well as can be expected.

In addition to the visual examination of the results, speedups were calculated for the parallel algorithm on all the presented domains. In Figure 12, speedups are shown with fixed $n_p = 4096000$ and varying p. The results reveal that there is very little difference between the 2-D and 3-D domains in terms of scalability. One pattern that emerges is that 2-D clover domain performs the worst and even that is only noticeable on 17 or more threads.

Although the complexity of the domain border, which dictates the time required to calculate Ω, should also influence the performance, this cannot be demonstrated on the presented domains. E.g., the performance does vary a lot on the 2-D maze with its

18

(a) 3-D clover

(b) 3-D heatsink

(c) 3-D bunny

(d) 3-D maze
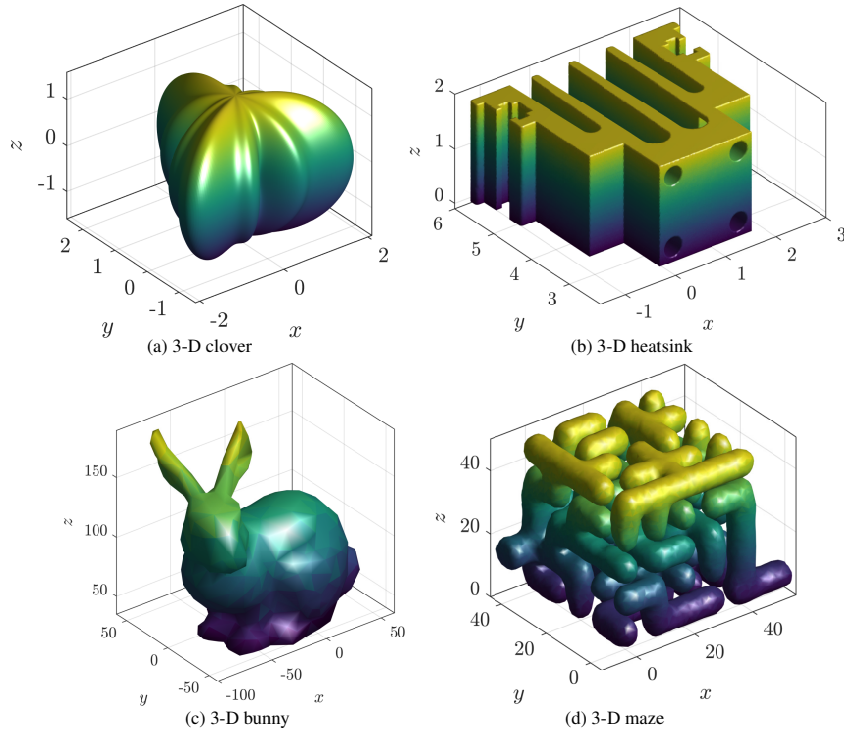
Figure 9: 3-dimensional test domains.

arguably most complex border shape due to the lack of dynamic load-balancing, but is generally distinctly better than the performance on the much simpler 2-D clover shape.

The overall result of the experiments presented in this section is that while the performance does depend on the domain shape and spacing function, it varies very little if only the physical cores of the computer are used. For better exploitation of the SMP, however, a dynamic load-balancing is likely required.

4.4. Quality of point placement

The presented algorithm's end goal is to use the generated points as nodes of a meshless numerical approach. The parallel version of the algorithm does not produce exactly the same node distributions as the sequential version. This may cause some concerns about the quality of the node distribution produced by the parallel version. However, the sequential version, run with the set of points obtained during the parallel algorithm's bootstrapping phase as the seed point set, will produce nearly the same point set as the parallel algorithm. The sequential algorithm produces good quality point distributions, provided that the given set of seed points is of sufficient quality, which is true in our case, as the sequential algorithm itself generated the seeds. Nonetheless, we compare some of the basic quality measures of node sets for numerical approaches, as used in [4] and [38].

Table 1: Different spacing functions for the presented domains.

2-D	$h_t(x, y) =$	
heatsink	h_s	(19)
clover	$h_s \left(1 + 4\cos^2(3\arg(x, y))\tanh(\sqrt{x^2 + y^2}) \right)$	(20)
bunny	$h_s \left((1 + y/100)^{1.5} \right)$	(21)
maze	$h_s \left((1 + y/20)^{1.5} \right)$	(22)
3-D	$h_t(x, y, z) =$	
heatsink	h_s	(23)
clover	$h_s \left(0.5 + \cos^2(3\arg(x, y) + \pi/3)\tanh((2 - z)\sqrt{x^2 + y^2 + z^2}) \right)$	(24)
bunny	$h_s (1 + (4 * (180 - z)/180))$	(25)
maze	$h_s (4 + \sin(x\pi/5))$	(26)

A basic measure of node quality is to check how well the distances to neighbouring nodes match the prescribed nodal spacing function h. We compute the distances $\{d_{i,j}\}_{i=1, j=1}^{N,k}$ for each node p_i to its k nearest neighbours (excluding p_i itself), and define the normalized distances $d'_{i,j} = d_{i,j}/h(p_i)$. A histogram of $d'_{i,j}$ is then plotted, with the expectation that most values are located around 1.

Such histograms are shown in figure 13 for the 2-D clover shape (6) with the nodal spacing function (7), with $h_{\min} = 0.0016$ and $h_{\max} = 0.0078$. There are some differences between the histograms of the sequential and parallel version, but they are an order of magnitude smaller than the actual counts, and both histograms represent acceptable node distributions.

Additionally, we can calculate the average distance to nearest neighbours $\bar{d}_i = \frac{1}{k}\sum_{j=1}^{k} d_{i,j}$, as well as the maximum and minimum distances to neighbours for each point:

$$d_i^{\min} = \min_{j=1,\ldots,k} d_{i,j}, \qquad d_i^{\max} = \max_{j=1,\ldots,k} d_{i,j}. \tag{27}$$

All these distances can be normalized by $h(p_i)$, to obtain $\bar{d}'$, $(d_i^{\min})'$, etc. Some statistics of $d_{i,j}$ are recorded in table 2. Both algorithms perform well, with the parallel version showing slightly more dispersed distances to nearest neighbours.

Additional quality measure, which often appears in convergence and stability proofs is quasi-uniformity [39], or in the case of variable nodal spacing h-quasi-uniformity [40]. Quasi-uniformity represents the notion that the relative distances between the neighbouring nodes are approximately equal for a sequence of node sets. Formally, it defines the "node set ratio" (analogous to mesh ratio) of a node set X covering Ω as a quotient

(a) 2-D clover

(b) 2-D heatsink

(c) 2-D bunny

(d) 2-D maze
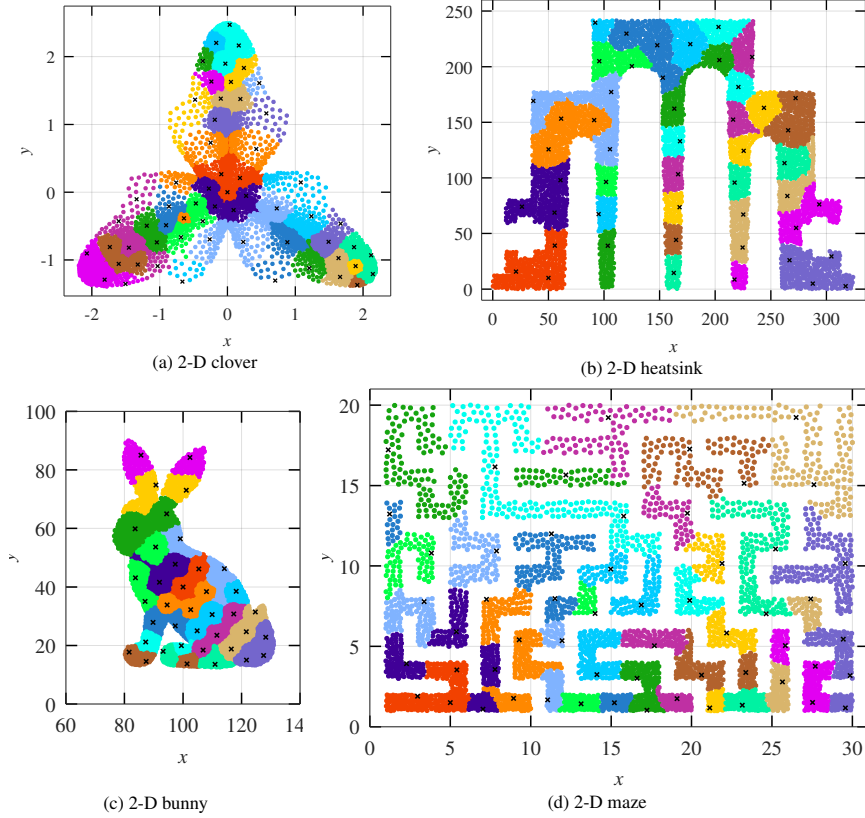
Figure 10: The 2-dimensional domains, filled with cell-based algorithm running on 16 threads. Points placed by different threads are coloured by different colours. While the variable spacing is clearly seen in the clover and maze domains, it is also indicated from the variable size of cells in the bunny domain, where spacing increases from bunny's feet and tail towards its head and ears.

of the "fill distance" and "separation distance":

$$\gamma_{X,\Omega,h} = \frac{\max_{p_i \in X} h_{X,\Omega}(p_i)/h(p_i)}{\min_{p_i \in X} s_X(p_i)/h(p_i)}, \tag{28}$$

where $h_{X,\Omega}(p)$ is the diameter of the largest empty ball in Ω that touches p, and $s_X(p)$ is the distance from p to its closest neighbour:

$$h_{X,\Omega}(p) = 2 \sup_{q \in \Omega}\{\|p - q\|, B(q, \|p - q\|) \cap X = \emptyset\}, \tag{29}$$

$$s_X(p) = \min_{q \in X\setminus\{p\}} \|p - q\|. \tag{30}$$

A sequence of node sets $(X_\lambda)_\lambda$ with nodal spacing functions h_λ is called quasi-uniform, if the node set ratios $\gamma_{X_\lambda,\Omega,h_\lambda}$ are uniformly bounded.

The node sets X_i were generated for the 2-D clover shape (6) with the nodal spacing

21

(a) 3-D clover

(b) 3-D bunny

(c) 3-D maze

(d) 3-D heatsink
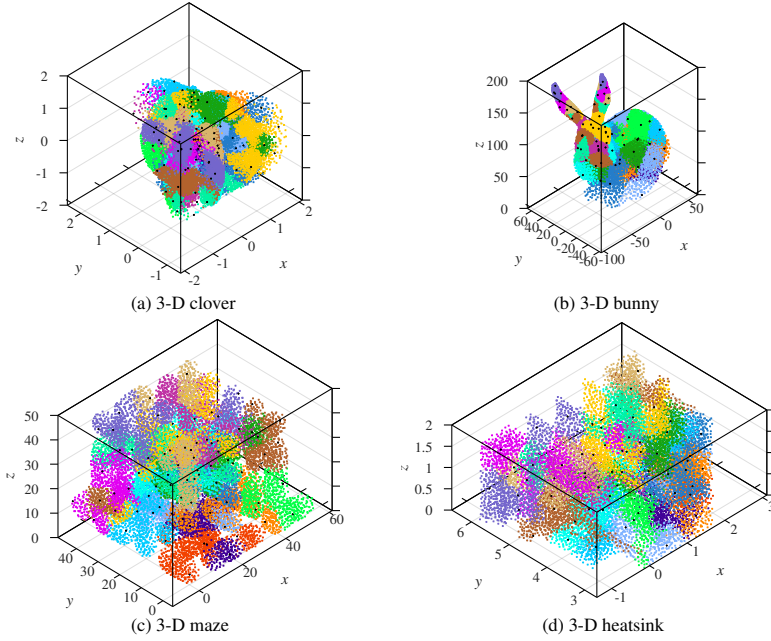
Figure 11: The 3-dimensional domains, filled with a cell-based algorithm running on 16 threads. Points placed by different threads are coloured by different colours.

Table 2: Numerical quantities related to local regularity.

algorithm	mean $\bar{d}_i'$	std $\bar{d}_i'$	mean $\left(\left(d_i^{\max}\right)' - \left(d_i^{\min}\right)'\right)$
sequential	1.1914	0.0586	0.5069
parallel	1.1905	0.0598	0.5076

function (7), with $(h_{\min})_i$ and $(h_{\max})_i$ as given as $(h_{\min})_i = 0.05/2^i$ and $(h_{\max})_i = 0.25/2^i$, for $i = 0, \ldots, 7$.

The values of $h_{X_i,\Omega,h_i} := \max_{p_j \in X_i} h_{X_i,\Omega}(p_j)/h_i(p_j)$ and $s_{X_i,h} := \min_{p_j \in X_i} s_{X_i}(p_j)/h_i(p_j)$ are shown in figure 14 for the node sets X_i. Both values share the same behaviour in the parallel and sequential versions of the algorithm, and it can be deduced from the figure that the node set ratio γ_{X_i,Ω,h_i} is bounded, indicating a node distribution of sufficient quality for PDE solving.

Additionally, the node distributions produced by the parallel and sequential versions of the algorithm are compared on a model boundary value problem with a manufactured solution, to asses any potential difference in errors or condition numbers that might appear. A Poisson problem on the 2-D clover domain Ω is considered, specifi-
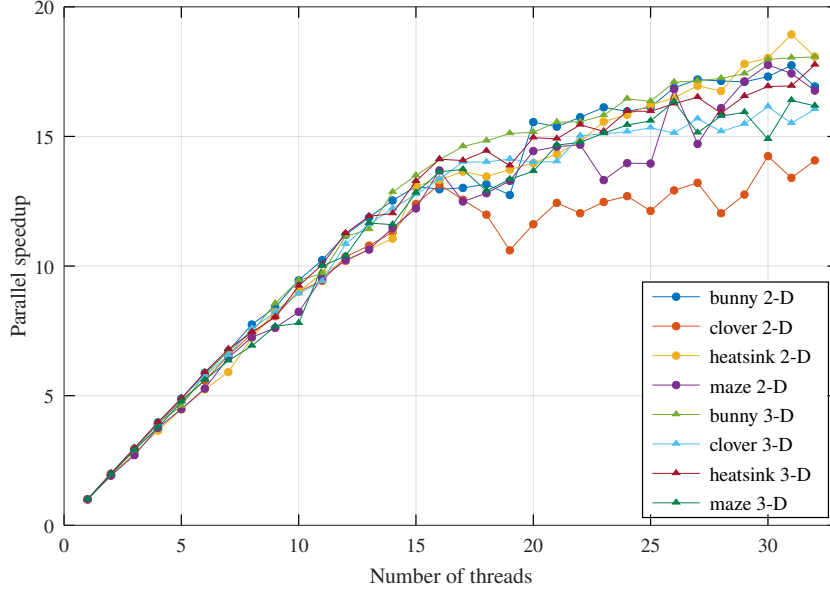
Figure 12: The speedup on various domain types.

cally

$$\nabla^2 u(x, y) = -\frac{2}{9}\pi^2 \sin(\pi x/3) \sin(\pi y/3) \qquad \text{in } \Omega, \qquad (31)$$

$$u(x, y) = \sin(\pi x/3) \sin(\pi y/3) \qquad \text{on } \partial\Omega, \qquad (32)$$

with the solution $u_a(x, y) = \sin(\pi x/3) \sin(\pi y/3)$.

The node sets were generated for the Clover-2D domain as before with spacing h as defined in table 1, in such a way that the number of nodes ranged between 1000 and 1000000. The numerical solution was obtained using RBF-FD method using PHS RBFs and monomial augmentation of 2nd order on stencils of 15 closest nodes.

The condition number $\kappa(M)$ of the final sparse matrix M was estimated using the Matlab's `condest` function, and the error was estimated by constructing a dense uniforms spaced grid of nodes G in the domain and comparing the difference between the numerical solution u_h and the closed-form solution u at the grid nodes. The differences were aggregated in two ways, giving estimates of the relative L_1, and L_∞ norms:

$$e_1 = \|u_h - u\|_1 / \|u\|_1, \quad \|f\|_1 = \frac{1}{|G|} \sum_{p \in G} |f(p)|, \qquad (33)$$

$$e_\infty = \|u_h - u\|_\infty / \|u\|_\infty, \quad \|f\|_\infty = \max_{p \in G} |f(p)|. \qquad (34)$$

The results are presented in figure 15 along with the growth rates. No major differences between parallel and sequential versions are observed.

23
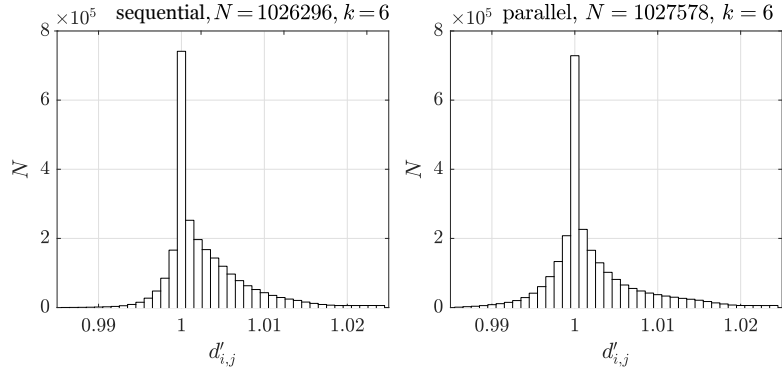
Figure 13: Histograms of normalized distances for sequential and parallel versions of the algorithm.
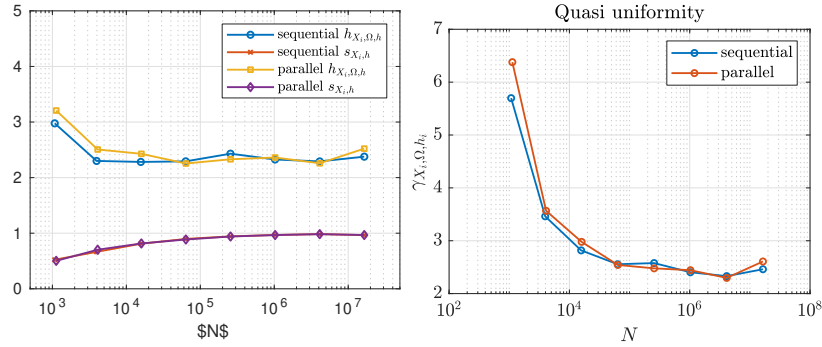
Figure 14: Quasi-uniformity analysis of the node sets generated on the 2-D clover domain. The left plot shows the normalized fill and separation distances, and the right plot shows the node set ratio.

5. Discussion

In this section we discuss the some of the approaches used in the algorithm and in the experiments.

5.1. Parallelization overhead

The parallel algorithm will always experience the overhead of creating, running and managing threads, which are the features not required by the sequential algorithm. It also experiences the overhead of the acquiring ownership of mutexes, which is again not required in the sequential version. This overhead could possibly be avoided with the use of non-locking thread-safe data structures, which is a direction for further improvements but is beyond the scope of this paper. These two overheads are demonstrated on the difference between the execution times of sequential algorithm and parallel algorithm with a single worker thread and no bootstrapping. The differences in execution times, normalised by the number of placed points for a clearer visualisation, are plotted in Figure 16. While there are both overheads present at all experiments, the thread management overhead should be more noticeable on the left part of the figure

24
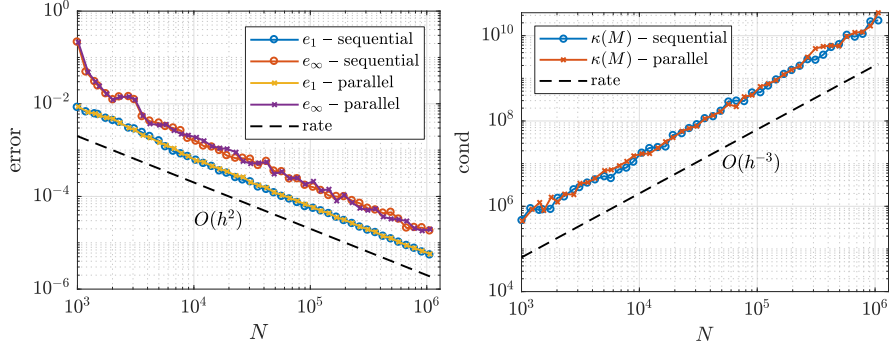
Figure 15: Comparison of estimated errors and condition numbers when solving a Poisson boundary value problem with nodal distributions generated by the parallel and sequential versions of the algorithm.

where the number of placed points is low, and the mutex overhead should dominate the right side of the figure where the number of placed points is high. The figure shows a the overhead to be very small, with no visible trend, and although averaged over 10 measurements, relatively noisy. Therefore, our overall observation is that the parallel overhead on our experimental system is about 400 ns, which is mostly due to the mutex acquisition, while the thread management overhead is negligible.

5.2. Iterative method for bootstrapping

Bootstrapping represents a method of generating a sufficient number of seed points for the parallel algorithm to load all the worker threads. The exact number of seed points, which should equal an integer multiple of the number of threads for best results, cannot be achieved easily. More than the requested number of points could be generated by bootstrapping and then reduced down to the desired number, but such reduction would degenerate the shape of cells induced by the seed points. According to our preliminary testing, it seems better to leave the number of seed points higher than requested and assign an unequal number of them to different threads.

There are multiple viable strategies for generating the required number of seed points, and the selection of an appropriate one could even be tailored to the specific use case. Below we only present a method that worked well for us and was used in all the experiments with bootstrapping in this article. That also means that its execution time was included in the execution times of the parallel algorithm runs. While the method is not optimal as it simply discards some results, which could potentially be refined; instead, its execution time is still insignificant compared to the whole algorithm.

The method takes the lower limit on the number of generated points as a parameter and guarantees as many or more will be generated. The main idea is to iterate over several values of the spacing amplification factor (see Section 3.1), until the obtained number of seed points is larger than the lower limit. The proposed method starts with spacing that is intentionally too high - i.e. the factor a is first estimated using 12, and multiplied by 10. Then in a loop, the point placement algorithm is executed with the current value for a, and the number of placed points is counted. While the target number of seed points is not reached, the loop repeats with the value of a halved. The
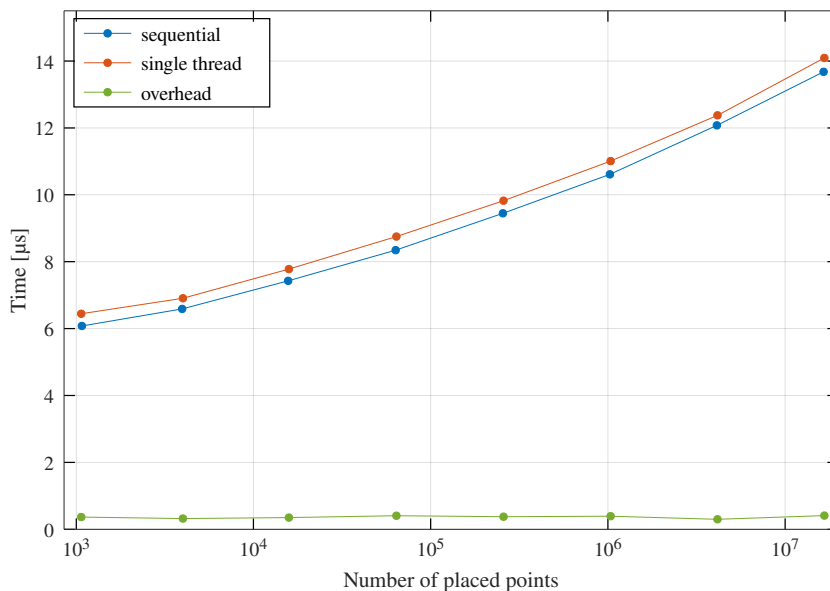
Figure 16: Comparison of the average time required for placing a single point between the sequential and parallel algorithms. Overhead is calculated as the difference between the two and comprises thread management and mutex ownership acquisition.

loop iterates until a sufficient number of points is generated. Bootstrapping is then complete, and the placed points are declared the seed points of the parallel algorithm.

5.3. Effects of Bootstrapping

Since the sequential algorithm does not require it, bootstrapping presents an overhead, but theoretically a relatively small one, since the total number of seed points relative to the total number of placed points is small. To see how significant this overhead is, we devised an experiment where we incrementally step up the number of generated seeds to numbers far beyond the required. Figure 17 displays how the number of seed points influences the speedup of the presented algorithm. It is plotted in a log–log form, for better visibility of speedups for low number of threads. All the experiments for this figure were executed on the clover domain, with $n_p = 4096000$, $n_c = 12$, and the same random seed for all executions. The latter ensures that even the influence of randomness is kept at a minimum. The number of seed points was aimed at multiples (1, 2, 3, 4, 6, 8, ... 20) of the maximum number of worker threads (32). In the figure, the obtained number of seed points (and thus cells) is listed since it reflects the overhead better than the requested number. The speedup was calculated as a time fraction relative to the original sequential algorithm, which does not perform bootstrapping but rather starts from a single seed point, placed at coordinates $(0, 0)$.

The low variation of results in the figure demonstrates the robustness of the placement algorithm to the number of cells; at least in combination with this particular domain and problem size. Only the lowest numbers of cells (60) results in visibly lower

26
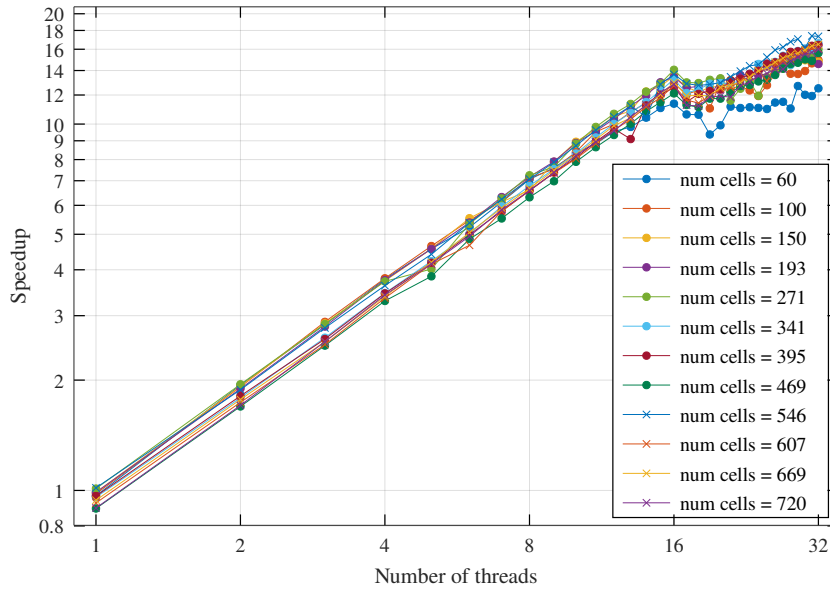
Figure 17: The speedup of the cell-based parallel algorithm as a function of the number of threads and the number of cells.

speedups across some range of experiments, while the others are clustered very closely. No clear pattern emerges for the other numbers of cells, and while some numbers of cells seem worse than others across the whole range, these are not the highest numbers, which are the ones with the highest bootstrapping overhead.

Furthermore, in the case of 546 cells, parallel algorithm executed on a single thread even outperforms the sequential algorithm. We have ensured that these results are not an error by repeating the tests several times. When dividing the domain between multiple cells and performing the search on a single thread with all the parallel algorithm's overheads, the parallel algorithm is still faster on average. Furthermore, whatever causes the divided domain to be filled faster, remains in effect even when the number of threads increases; regardless of the number of threads, the division into 546 cells results is one of the fastest executions for a given number of threads.

For a closer look at what defines the performance, we checked whether the cause was in static load balancing. Looking at the load balance expressed as the average ratio of idle versus work time for threads, we saw the loads were, in general, not balanced, but there was no correlation with the execution time. We only noticed that the sum of execution times of individual threads varies with the number of cells. To get more insight into what might be the cause of varying execution times, we show the single-thread execution time and the sum of all thread execution times for the 16-threaded execution in Figure 18. The obvious correlation between the execution times is not coincidental. If the execution on 16-threads were compensated for the parallel overhead, the two plotted curves would match almost perfectly. Since we ran the experiments

with a constant random seed, we obtained identical distributions of seed points for all the tests with the same number of seed points. It can be reasoned then that the execution times depend mainly on the shape of the indexing tree, governed the shape of its top level, which was in our case uniquely prescribed by the number of seed points but in general depends on seed point positions. It can be reasoned then that the correlation in execution times stems form the use of the dynamically built *k*-d tree as the spatial indexing method. Such a tree is generally not perfectly balanced, and the extent to which it is unbalanced in our case depends not only on chance but also on the distribution of seed points. Therefore, a viable option for future work is the research into other spatial indexing methods, and how the algorithm could benefit from them.
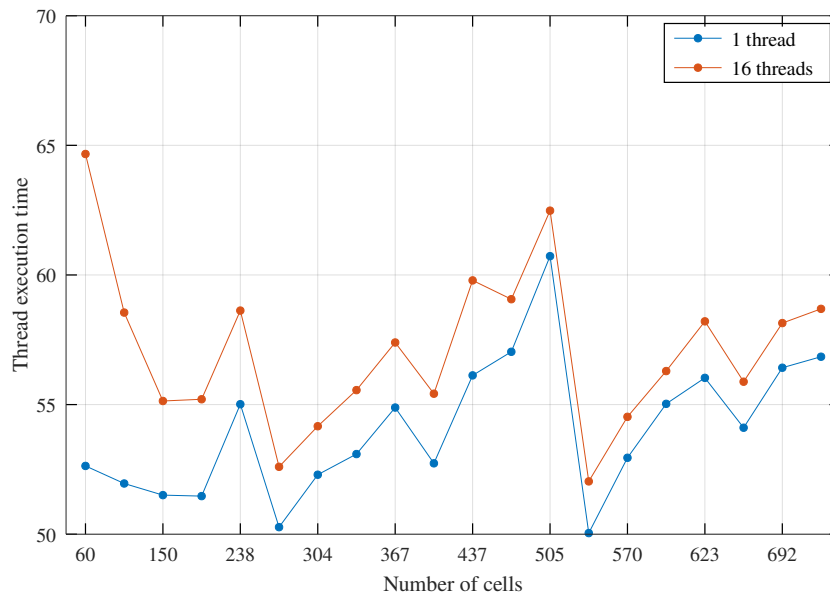
Figure 18: The single-threaded execution times contrasted to the sum of individual thread execution times on 16 threads. Markers represent the experiments while the lines are added only to aid the visual comparison of the variations within the two sets of experiments.

5.4. Points placed near cell borders

There are limitations to cell-based parallel approach beyond the already mentioned minimum number of seed points. One is also the proximity testing within individual cells. There can always appear pairs of points from neighbouring cells that would fail it, so some testing between neighbouring cells is required. Neighbouring cells are all those that can theoretically interfere with the point placement. To eliminate the chance of such pairs appearing, two methods have been considered:

- Testing for minimal distance within the neighbouring cells while placing points. If the candidate passes the proximity test in the parent cell it then has to be tested also in all the neighbouring cells. Those tests have to be done while all the

28

involved cells are locked for reading and writing, otherwise race condition could occur; i.e., another thread could theoretically attempt a similar action on an own candidate point, both threads might find the placement non-conflicting and then insert, each thread into another cell, a conflicting pair of points.

- Inserting all the points without checks in the neighbouring cells, but flagging flagging points that could cause a conflict conflict in the neighbouring cell, e.g., adding them to a list of points requiring additional checks in post-processing. After the placement is complete, all the flagged points must be checked for conflicts, and the actual conflicts solved, i.e. removing one of the conflicting points from the domain. Checking must be done systematically though, to properly deal with cases where one point appears in more than one conflict. And if done in parallel, it again has to be protected against race conditions.

Both methods require that testing of a candidate point comprises of finding two or more nearest cells – one to act as the parent cell, and others to check for possible interference with the candidate placement. Both methods also introduce additional overheads. We opted to use the first method for its greater simplicity but are considering the second one as future work.

The selected method introduces the overhead of checking for neighbours in more than one cell for all candidates on cell boundaries. The greater the area of boundaries relative to the total domain area, the greater the overhead of extra checking will be. We can experimentally evaluate the overhead, by varying the number of cells, and thus vary the ratio of cell boundary area relative to the total domain area. Experiments can even be done on a single thread to isolate the tested parameter form all the non-determinism of running in parallel. The execution of algorithm on a single thread for varying number of cells was already shown in Figure 17. Instead of seeing a pattern of increased execution time with the increasing area of cell borders, the experiment shows noise. Therefore, while we still expect the overhead to be there, it seems to be completely lost in other more significant factors to the overall execution time. For the time being, we consider this overhead too insignificant to be worth further analysis.

6. Conclusion

Parallelisation of the Poisson disc sampling algorithm for domain discretisation is attempted by running several sequential algorithm instances on a shared set of placed points and a shared spatial indexing method. The instances are executed on a shared-memory machine as threads. The main focus is put into sharing the data efficiently with minimal synchronisation overhead. To this end, the shared spatial indexing method (i.e. k-d tree) is implemented with a location-aware locking mechanism. A static load balancing mechanism is implemented through the generation of sub-domains or cells, and the use of thread-local sets of candidate points. Such load-balancing guides the threads to work on distant and compact sub-domains, and decreases the chances of conflicting access to the shared data.

The implementation is experimentally tested on several irregular domains with uniform and non-uniform nodal spacing functions. The experiments show that the parallel

algorithm is capable of high speedups. Moreover, its performance is not influenced by the geometric complexity of the domain. Additionally, the experimental analysis of the presented parallelisation approach includes the costs of various overheads and produces ideas for future work.

The main limitation of the algorithm is in its use of dynamically constructed k-d tree, which can become arbitrarily unbalanced and thus cause larger than necessary search times. Different spatial indexing strategies will be considered for replacing the k-d tree. There is also an array of improvements that could be made in handling border nodes. The existing border nodes should be exploited to increase the number of concurrent moving fronts and thus contribute to a more efficient parallelization. Processing the border nodes within the cellular structure, however, requires careful development and analysis to avoid extensive overheads that would make such an endeavour counterproductive.

In future, besides addressing the deficiencies mentioned above we will focus on two additional aspects. First, how to implement a distributed variant of the discussed algorithm. Second, how to utilize the presented parallel node generation algorithm to generate balanced sub-domains for the domain decomposition.

7. Acknowledgements

References

[1] R. Trobec, G. Kosec, Parallel scientific computing: theory, algorithms, and applications of mesh based and meshless methods, Springer, 2015.

[2] G.-R. Liu, Mesh free methods: moving beyond the finite element method, CRC press, 2002. `doi:10.1201/9781420040586`.

[3] T. Jacquemin, S. Tomar, K. Agathos, S. Mohseni-Mofidi, S. P. A. Bordas, Taylor-series expansion based numerical methods: A primer, performance benchmarking and new approaches for problems with non-smooth solutions, Archives of Computational Methods in Engineering 27 (5) (2020) 1465–1513. `doi:10.1007/s11831-019-09357-5`.

[4] J. Slak, G. Kosec, On generation of node distributions for meshless PDE discretizations, SIAM Journal on Scientific Computing 41 (5) (2019) A3202–A3229. `doi:10.1137/18m1231456`.

[5] O. C. Zienkiewicz, R. L. Taylor, J. Z. Zhu, The finite element method: its basis and fundamentals, Elsevier, 2005.

[6] D. P. Hardin, E. B. Saff, Discretizing manifolds via minimum energy points, Notices of the AMS 51 (10) (2004) 1186–1194.

[7] G. Kosec, A local numerical solution of a fluid-flow problem on an irregular domain, Adv. Eng. Software 120 (2018) 36–44. `doi:10.1016/j.advengsoft.2016.05.010`.

[8] Y. Liu, Y. Nie, W. Zhang, L. Wang, Node placement method by bubble simulation and its application, Computer Modeling in Engineering and Sciences (CMES) 55 (1) (2010) 89. `doi:10.3970/cmes.2010.055.089`.

[9] R. Löhner, E. Oñate, A general advancing front technique for filling space with arbitrary objects, Int. J. Numer. Methods Eng. 61 (12) (2004) 1977–1991. `doi:10.1002/nme.1068`.

[10] X.-Y. Li, S.-H. Teng, A. Ungor, Point placement for meshless methods using sphere packing and advancing front methods, in: ICCES'00, Los Angeles, CA, Citeseer, 2000.

[11] R. L. Cook, Stochastic sampling in computer graphics, ACM Trans. Graphics 5 (1) (1986) 51–72. `doi:10.1145/7529.8927`.

[12] V. Shankar, R. M. Kirby, A. L. Fogelson, Robust node generation for meshfree discretizations on irregular domains and surfaces, SIAM J. Sci. Comput. 40 (4) (2018) 2584–2608. `doi:10.1137/17m114090x`.

[13] B. Fornberg, N. Flyer, A primer on radial basis functions with applications to the geosciences, SIAM, 2015. `doi:10.1137/1.9781611974041`.

[14] J. Slak, G. Kosec, Adaptive radial basis function–generated finite differences method for contact problems, International Journal for Numerical Methods in Engineering 119 (7) (2019) 661–686. `doi:10.1002/nme.6067`.

[15] J. Slak, G. Kosec, Medusa: A C++ library for solving PDEs using strong form mesh-free methods, ACM Transactions on Mathematical Software `http://e6.ijs.si/medusa/` (2021).

[16] M. Jančič, J. Slak, G. Kosec, Monomial augmentation guidelines for RBF-FD from accuracy versus computational time perspective, Journal of Scientific Computing 87 (1) (feb 2021). `doi:10.1007/s10915-020-01401-y`.

[17] M. Maksić, V. Djurica, A. Souvent, J. Slak, M. Depolli, G. Kosec, Cooling of overhead power lines due to the natural convection, International Journal of Electrical Power & Energy Systems 113 (2019) 333–343. `doi:10.1016/j.ijepes.2019.05.005`.

[18] U. Duh, G. Kosec, J. Slak, Fast variable density node generation on parametric surfaces with application to mesh-free methods, SIAM Journal on Scientific Computing 43 (2) (2021) A980–A1000. `doi:10.1137/20m1325642`.

[19] K. P. Drake, E. J. Fuselier, G. B. Wright, Implicit surface reconstruction with a curl-free radial basis function partition of unity method, arXiv preprint arXiv:2101.05940 (2021).

[20] M. Thimnejad, N. Fallah, A. R. Khoei, Adaptive refinement in the meshless finite volume method for elasticity problems, Computers & Mathematics with Applications 69 (12) (2015) 1420–1443. `doi:10.1016/j.camwa.2015.03.023`.

[21] A. Angulo, L. P. Pozo, F. Perazzo, A posteriori error estimator and an adaptive technique in meshless finite points method, Engineering Analysis with Boundary Elements 33 (11) (2009) 1322–1338. `doi:10.1016/j.enganabound.2009.06.004`.

[22] O. C. Zienkiewicz, J. Z. Zhu, A simple error estimator and adaptive procedure for practical engineerng analysis, International Journal for Numerical Methods in Engineering 24 (2) (1987) 337–357. `doi:10.1002/nme.1620240206`.

[23] D. T. Oanh, O. Davydov, H. X. Phu, Adaptive rbf-fd method for elliptic problems with point singularities in 2d, Applied Mathematics and Computation 313 (2017) 474–497. `doi:10.1016/j.amc.2017.06.006`.

[24] P. Sang-Hoon, K. Kie-Chan, Y. Sung-Kie, A posterior error estimates and an adaptive scheme of least-squares meshfree method, International Journal for Numerical Methods in Engineering 58 (8) (2003) 1213–1250. `doi:10.1002/nme.817`.

[25] J. Slak, Partition-of-unity based error indicator for local collocation meshless methods, in: 2021 44rd International Convention on Information, Communication and Electronic Technology (MIPRO), IEEE, 2021, pp. 280–284.

[26] O. Davydov, D. T. Oanh, Adaptive meshless centres and RBF stencils for Poisson equation, Journal of Computational Physics 230 (2) (2011) 287–304. `doi:10.1016/j.jcp.2010.09.005`.

[27] G. Kosec, B. Šarler, H-adaptive local radial basis function collocation meshless method, CMC: Computers, Materials & Continua 26 (3) (2011) 227–253. `doi:10.3970/cmc.2011.026.227`.

[28] T. Jacquemin, S. P. A. Bordas, A unified algorithm for the selection of collocation stencils for convex, concave, and singular problems, International Journal for Numerical Methods in Engineering 122 (16) (2021) 4292–4312.

[29] L.-y. Wei, Parallel Poisson disk sampling, ACM Trans. Graphics (2008). `doi:10.1145/1399504.1360619`.

[30] X. Ying, S.-Q. Xin, Q. Sun, Y. He, An intrinsic algorithm for parallel Poisson disk sampling on arbitrary surfaces, IEEE transactions on visualization and computer graphics 19 (2013) 1425–1437. `doi:10.1109/TVCG.2013.63`.

[31] X. Li, S. Li, A linearized element-free galerkin method for the complex ginzburg–landau equation, Computers & Mathematics with Applications 90 (2021) 135–147.

[32] J. Slak, G. Kosec, Medusa: a c++ library for solving pdes using strong form mesh-free methods, ACM Transactions on Mathematical Software (TOMS) 47 (3) (2021) 1–25.

[33] M. Zoll, Heatsink, GrabCAD community, file: Heatsink.stl (May 2012).
URL `https://grabcad.com/library/heatsink--1`

[34] M. Raynal, Concurrent programming: algorithms, principles, and foundations, Springer Science & Business Media, 2012.

[35] J. L. Blanco, P. K. Rai, nanoflann: a C++ header-only fork of FLANN, a library for nearest neighbor (NN) with KD-trees (2014).
URL `https://github.com/jlblancoc/nanoflann`

[36] OpenGP, Watertight Stanford Bunny, file: bunny.off (Jan. 2014).
URL `https://github.com/OpenGP/OpenGP/blob/master/data/bunny.off`

[37] C. Patrick, 3d-maze-generator (2017).
URL `https://github.com/conorpp/3d-maze-generator`

[38] K. van der Sande, B. Fornberg, Fast variable density 3-D node generation, SIAM Journal on Scientific Computing 43 (1) (2021) A242–A257. `doi:10.1137/20M1337016`.

[39] H. Wendland, Scattered data approximation, no. 17 in Cambridge Monographs on Applied and Computational Mathematics, Cambridge University Press, 2004. `doi:10.1017/cbo9780511617539`.

[40] J. Slak, Adaptive RBF-FD method, Ph.D. thesis, University of Ljubljana (2020).